Supplementary Material

Self-supporting Fe, Co co-doped Ni_3S_2 nanosheet arrays as advanced bifunctional electrocatalysts for alkaline seawater splitting

Hao Zhang[a,b]†, Xinxiang Pei[c]†, Junwei Chen[a,b], Hanming Zhang[d], Wangzhi Zhang[d], Junyang Ding[a,b], Peipei Jia[b]*, Longcaho Zhuo[e], Xijun Liu[c]*, and Jun Luo[b]*

[a] *University of Electronic Science and Technology of China, Chengdu 611731, China*

[b] *ShenSi Lab, Shenzhen Institute for Advanced Study, University of Electronic Science and Technology of China, Longhua District, Shenzhen 518110, China*

[c] *Guangxi Key Laboratory of Processing for Non-ferrous Metals and Featured Materials, MOE Key Laboratory of New Processing Technology for Nonferrous Metals and Materials, School of Resources, Environment and Materials, Guangxi University, Nanning 530004, Guangxi, China*

[d] *Oil & Gas Technology Research Institute of Qinghai Oilfield Company, CNPC, Jinda East Road, Qili Town, Dunhuang, Jiuquan, Gansu 736202, China*

[e] *School of Materials Science and Engineering, Xi'an University of Technology, Xi'an 710048, China*

Authors to whom correspondence should be addressed: junyangdingde18@163.com, jiapeipei@uestc.edu.cn, xjliu@gxu.edu.cn

† These authors contributed equally.

Experimental Section

Materials

Iron nitrate nonahydrate ($Fe(NO_3)_3 \cdot 9H_2O$, AR), cobalt nitrate hexahydrate ($Co(NO_3)_2 \cdot 6H_2O$, AR, 99%), nickel nitrate hexahydrate ($Ni(NO_3)_2 \cdot 6H_2O$, AR, 98%), ammonium fluoride (NH_4F, AR, 98%), and urea ($CO(NH_2)_2$, AR, 99%), Ruthenium(IV) oxide (RuO_2, ≥98.0 %) and Ethanol (C_2H_5OH, ≥99.7 %) are purchased from Aladdin. Sodium sulfide nonahydrate ($Na_2S \cdot 9H_2O$, ≥98.0 %) is taken from Macklin. Acetone, concentrated hydrochloric acid, and potassium hydroxide (KOH, GR) are purchased from Sinopharm Chemical Reagent Co., Ltd. Natural seawater (pH=7.90) is obtained from the Yellow Sea, China. Platinum on carbon (PtC, 20 wt.%) and Nafion solution (5 wt.%) are from Hesen. Distilled water with a resistivity higher than 18 MΩ·cm was used throughout the experiments. Nickel foam (2 mm thick, 110 ppi pore size) purchased from Yiminglong.

Characterizations

X-ray diffraction (XRD) measurements were performed in the 2θ range of 10~80° on a Bruker D8 diffractometer operated at 40 kV and 40 mA with Cu Kα radiation to identify the crystalline phases. The surface morphology was characterized by scanning electron microscopy (SEM, FEI Quanta FEG 250) and transmission electron microscopy (TEM, FEI Talos F200X). Elemental distribution in selected regions was examined using a TEM equipped with energy-dispersive X-ray (EDX) for elemental mapping. The surface composition and chemical states were investigated by X-ray photoelectron spectroscopy (XPS) on a Thermo Fisher Scientific ESCALAB 250Xi system employing Al Kα radiation, and all binding energies were calibrated against the C 1s peak at 284.8 eV. The pH values of all electrolytes used in this work were obtained using a pH meter (Lei--Ci, PHS-3E).

Electrochemical tests

The electrochemical measurements for HER/OER (1 M KOH + natural seawater, pH=13.80) were performed on a CHI 760E electrochemical workstation employing a conventional three-electrode configuration. A graphite rod (6.0 mm diameter) served as the counter electrode, while a Hg/HgO electrode (in 1 M KOH) was used as the reference electrode. The self-supporting electrodes (S-FeCoNi/NF-1.0, S-FeCoNi/NF-0.5, S-FeCoNi/NF-1.5, FeCoNi/NF, and S-NF) can be directly used as the working electrode for testing without further processing. Commercially available powdered catalysts (20 wt.% Pt/C and RuO_2) require drop-casting onto a nickel foam (NF) conductive substrate to prepare the corresponding active electrodes. Specifically, a catalyst ink was prepared by dispersing 5 mg of catalyst powder in a mixed solution of 450 μL ethanol and 50 μL of 5 wt.% Nafion, followed by ultrasonication for 60 min in an ice-water bath to ensure uniform dispersion. Next, 100 μL was drop-coated onto a clean NF (2 mm thick; 110 ppi pore size; 1.0 ×2.0 cm^2; working area: 1.0 ×1.0 cm^2), and the catalyst-coated substrate was dried under an infrared lamp for 30 min prior to reserve.

All measured potentials were converted to the reversible hydrogen electrode (RHE) scale according to the Nernst equation ($E_{RHE} = E_{Hg/HgO} + 0.059 \times pH + 0.098$ V), and 90% IR compensation was applied. Linear sweep voltammetry (LSV) was conducted at a scan rate of 5 mV s^{-1}. Electrochemical impedance spectroscopy (EIS) measurements were performed over a frequency range of 0.1 Hz to 100 kHz with an amplitude of 5 mV at an overpotential of 100 mV. The double-layer capacitance (C_{dl}) was determined from cyclic voltammetry (CV) curves collected within the non-Faradaic potential region to estimate the electrochemically active surface area (ECSA). Long-term stability was evaluated by chronoamperometry (CP) at a constant current density of 100 mA cm^{-2}. For the integrated HER||OER configuration used to measure the volume of hydrogen and oxygen produced, a gas-tight H-type electrolytic cell equipped with an anion-exchange membrane (FAS-PET-130, fumasep) was employed to separate the cathodic and anodic compartments.

TOF measurements

The turnover frequency (TOF) values were calculated according to the previously reported equation [1]:

$$TOF = j / (n \times F \times N)$$

Where j is the current density; n is the electron transfer number; and F is the Faraday constant (96485 C mol^{-1}).

The N values were the number of active centers measured by a widely used method [2]: Cyclic voltammetry (CV) measurements were performed when the scan rate was fixed at 50 mV s^{-1}. After this, by integrating the charge of the CV curve over the whole potential range, the half value of the charge was obtained, which is the value of the surface charge density (Q_S). Then, the N value was calculated using the following equation:

$$N = Q_S / F$$

where F is the Faraday constant (96485 C mol^{-1}).

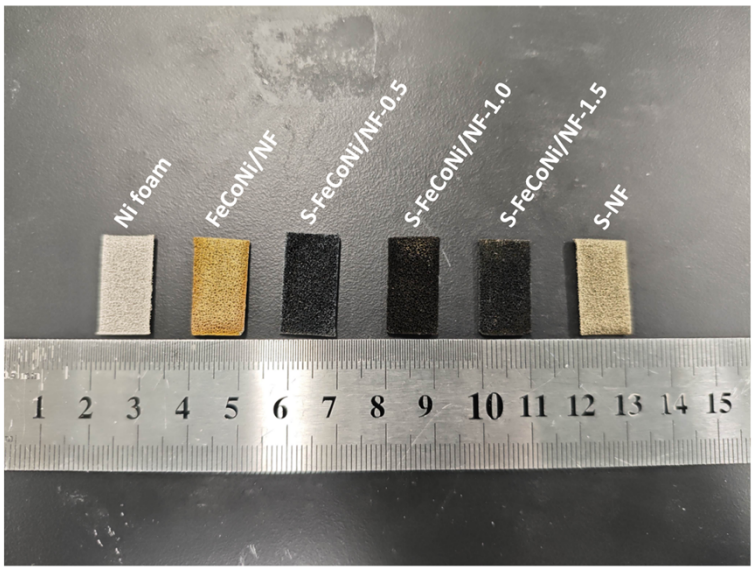

Figure S1. Optical images of the as-prepared samples.

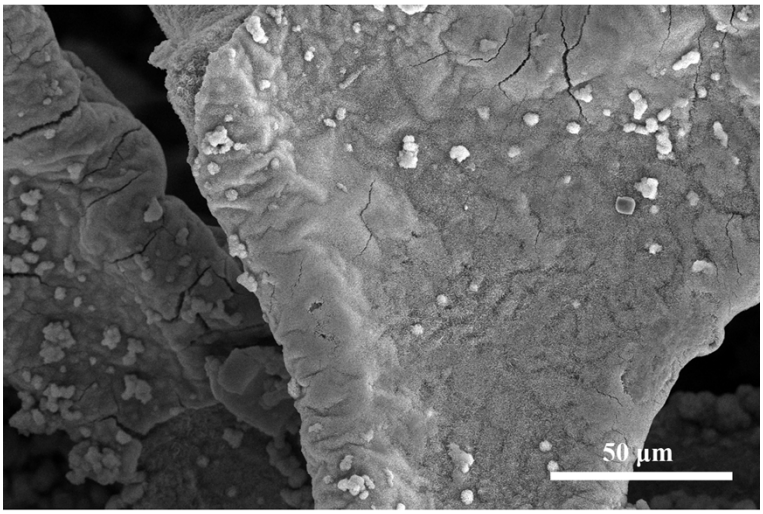

Figure S2. SEM images of the as-prepared FeCoNi/NF.

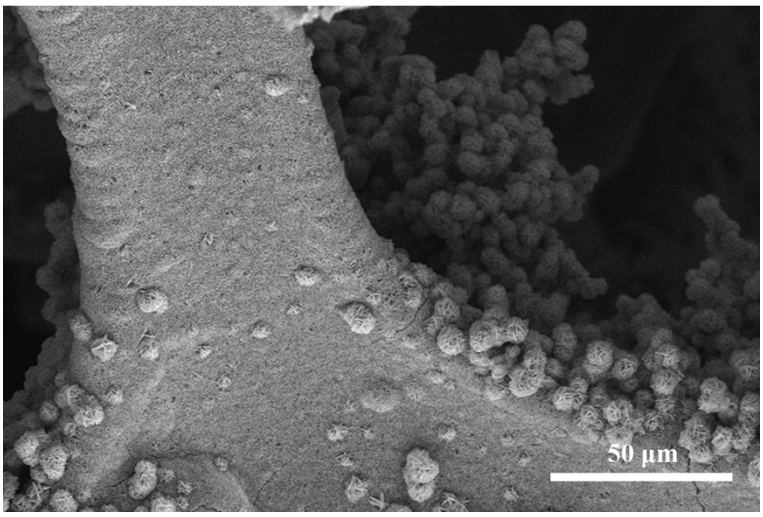

Figure S3. SEM images of the as-prepared S-FeCoNi/NF-1.0.

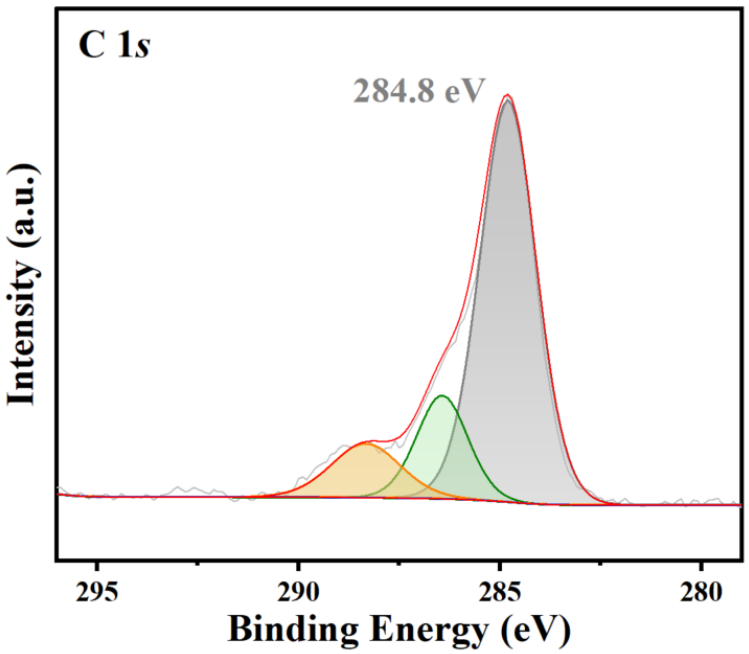

Figure S4. High-resolution C 1*s* XPS spectra of S-FeCoNi/NF-1.0.

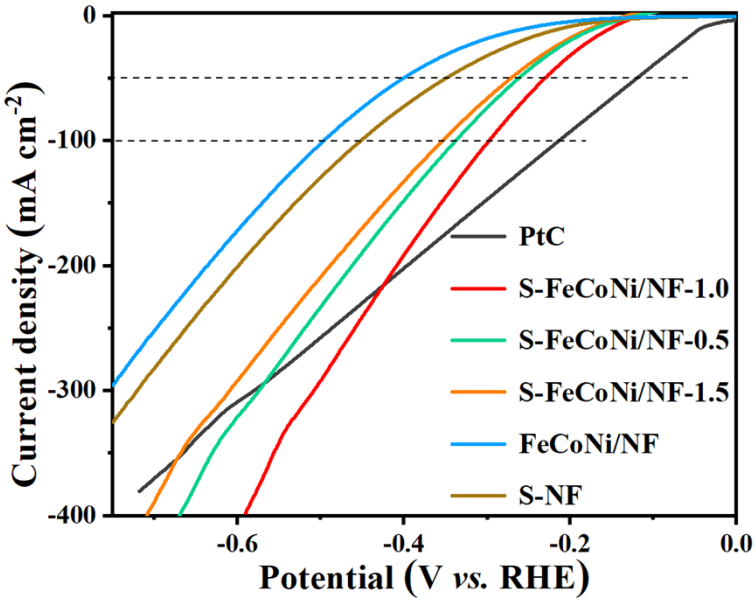

Figure S5. HER LSV curves of PtC, S-FeCoNi/NF-1.0, S-FeCoNi/NF-0.5, S-FeCoNi/NF-1.5, FeCoNi/NF, and S-NF without IR compensation.

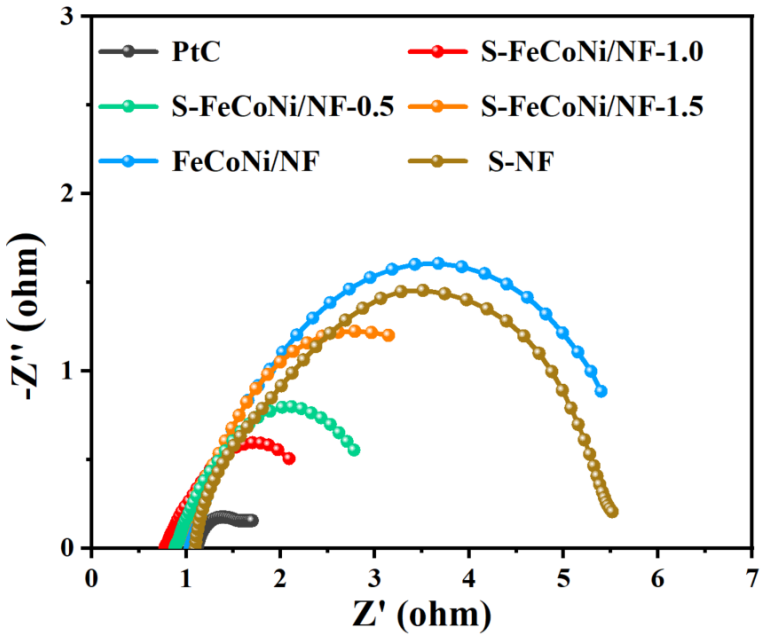

Figure S6. Nyquist profiles of PtC, S-FeCoNi/NF-1.0, S-FeCoNi/NF-0.5, S-FeCoNi/NF-1.5, FeCoNi/NF, and S-NF for HER.

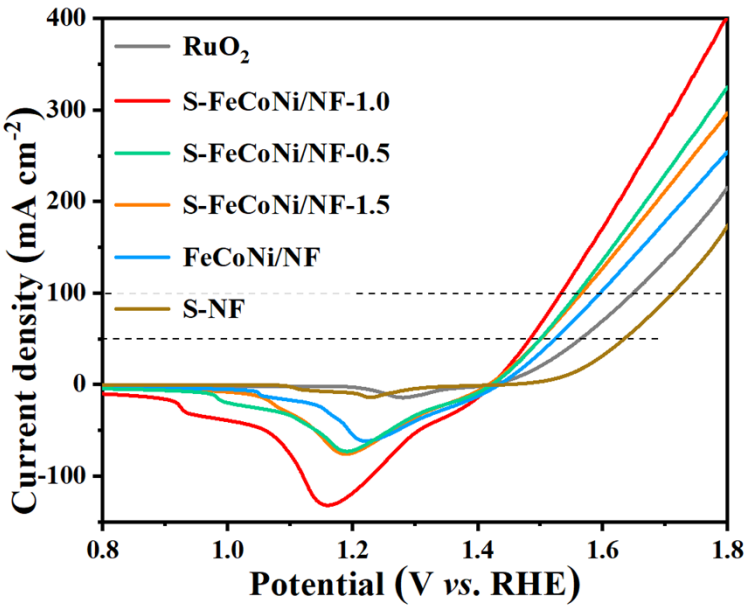

Figure S7. OER LSV curves of RuO_2, S-FeCoNi/NF-1.0, S-FeCoNi/NF-0.5, S-FeCoNi/NF-1.5, FeCoNi/NF, and S-NF without IR compensation.

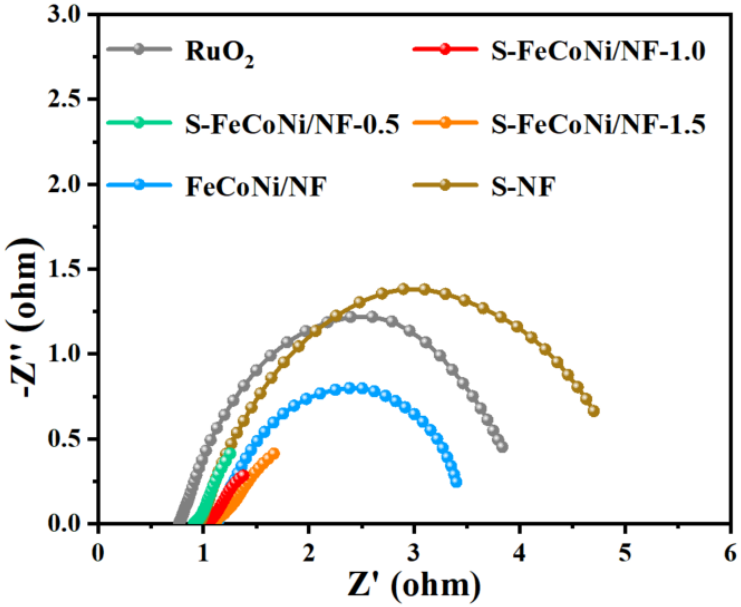

Figure S8. Nyquist profiles of PtC, S-FeCoNi/NF-1.0, S-FeCoNi/NF-0.5, S-FeCoNi/NF-1.5, FeCoNi/NF, and S-NF for OER.

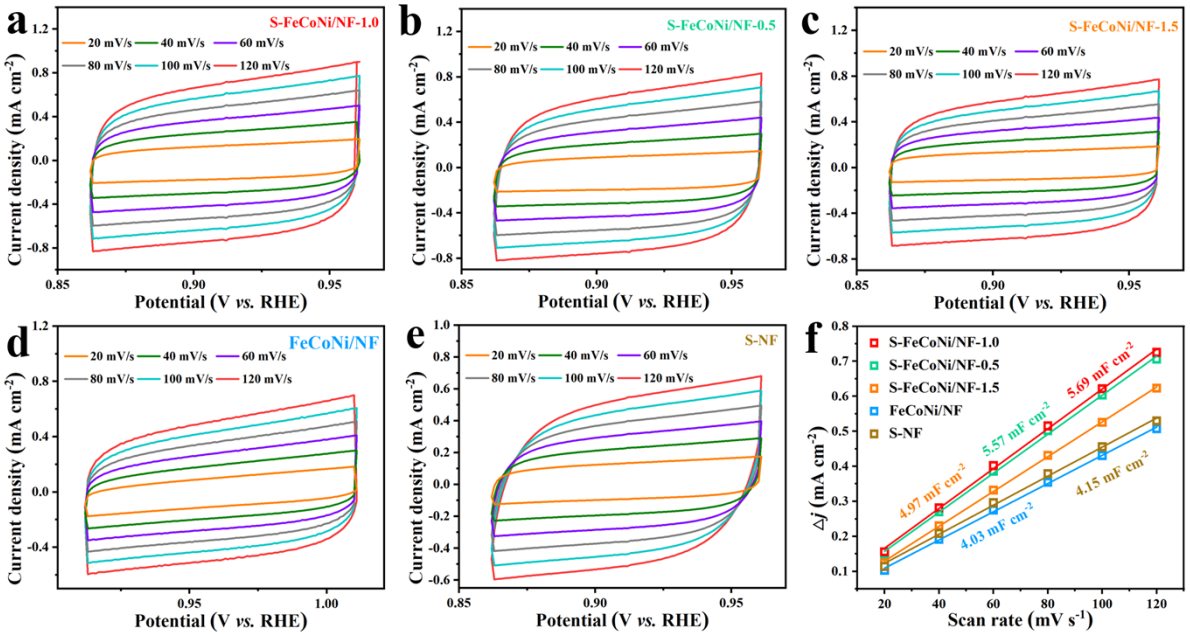

Figure S9. The CV curves at different scanning rates from 20 to 120 mV s^{-1} for (a) S-FeCoNi/NF-1.0, (b) S-FeCoNi/NF-0.5, (c) S-FeCoNi/NF-1.5, (d) FeCoNi/NF, and (e) S-NF. (f) The C_{dl} estimated from the scanning rate dependent CV curves.

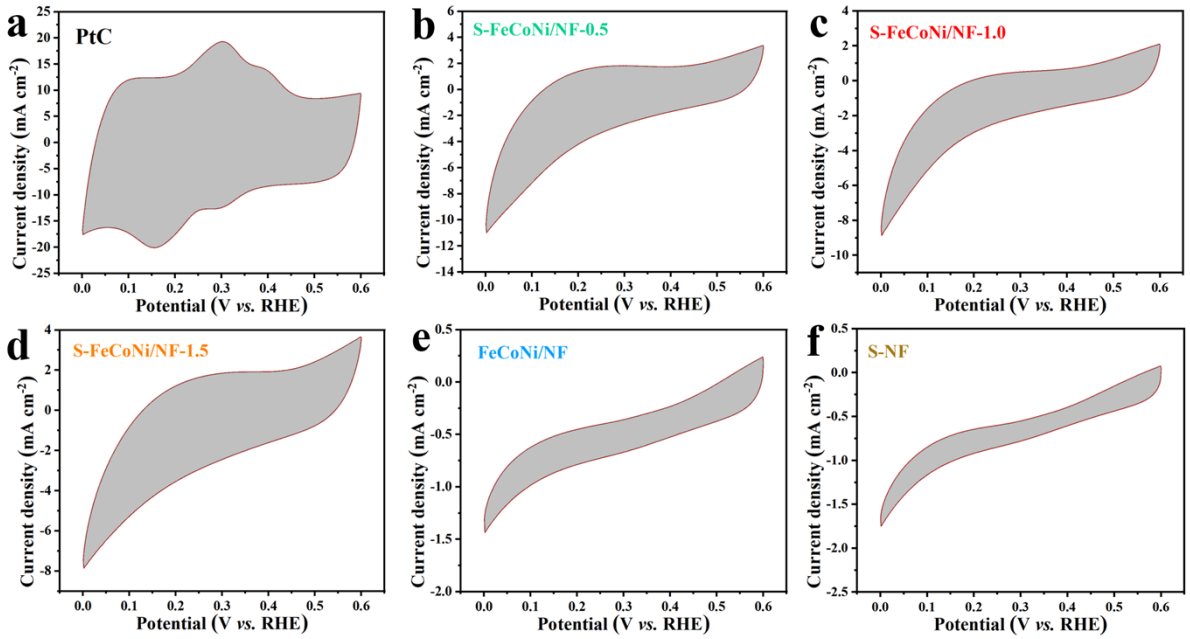

Figure S10. CV curves at 50 mV s^{-1} for PtC, S-FeCoNi/NF-0.5, S-FeCoNi/NF-1.0, S-FeCoNi/NF-1.5, FeCoNi/NF, and S-NF.

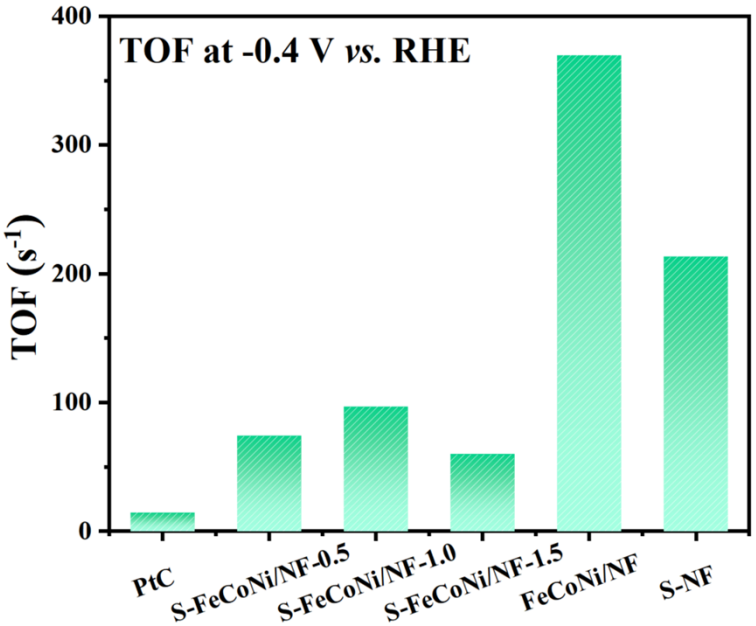

Figure S11. The calculated HER TOF values for PtC, S-FeCoNi/NF-0.5, S-FeCoNi/NF-1.0, S-FeCoNi/NF-1.5, FeCoNi/NF, and S-NF.

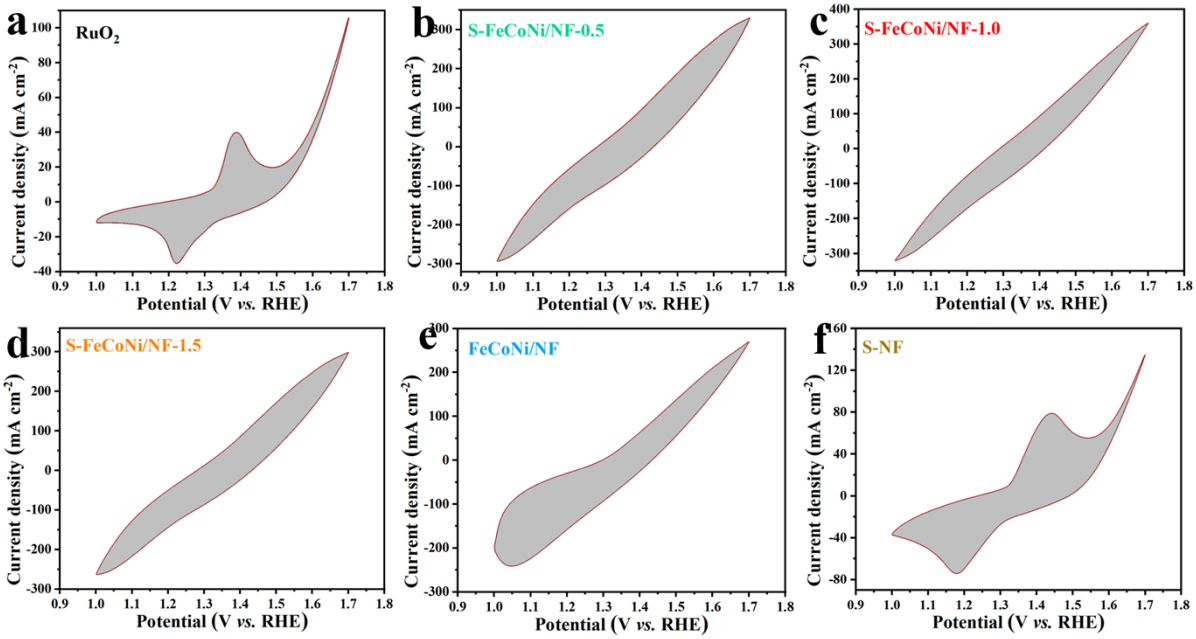

Figure S12. CV curves at 50 mV s^{-1} for RuO_2, S-FeCoNi/NF-0.5, S-FeCoNi/NF-1.0, S-FeCoNi/NF-1.5, FeCoNi/NF, and S-NF.

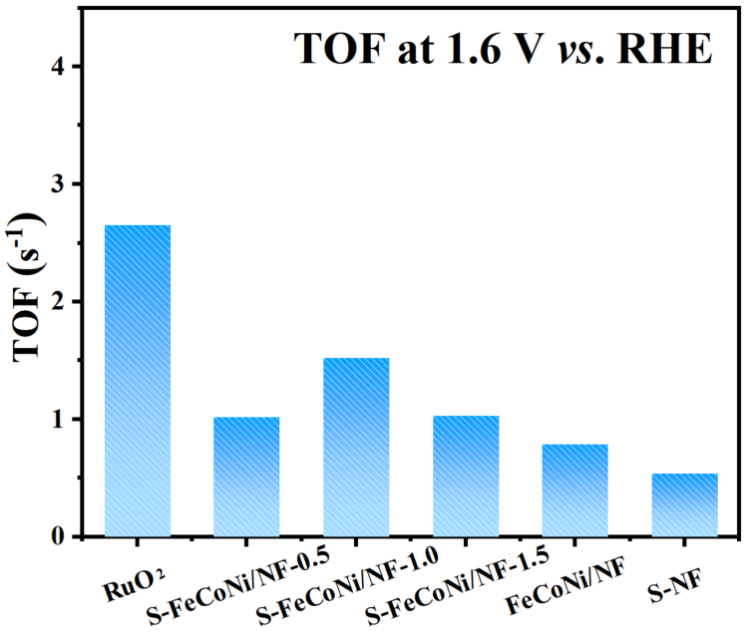

Figure S13. The calculated OER TOF values for RuO_2, S-FeCoNi/NF-0.5, S-FeCoNi/NF-1.0, S-FeCoNi/NF-1.5, FeCoNi/NF, and S-NF.

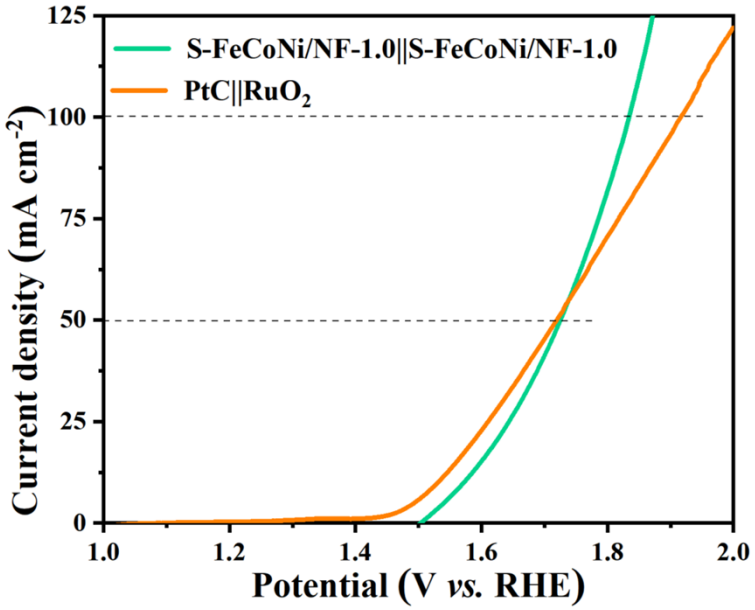

Figure S14. LSV curves of HER||OER alkaline seawater splitting systems without IR compensation.

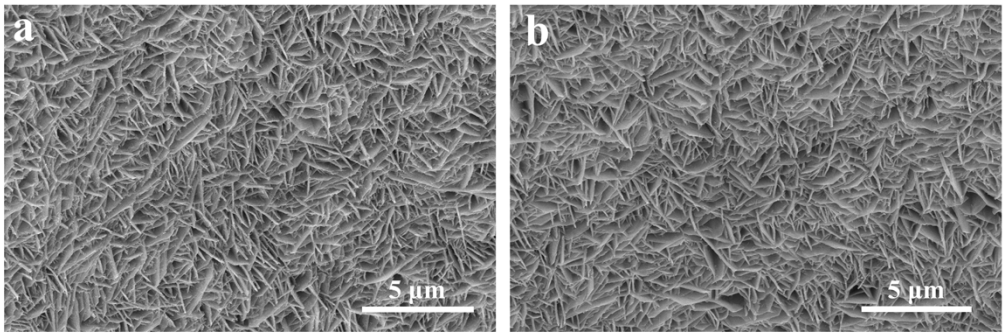

Figure S15. (a) and (b) SEM images of S-FeCoNi/NF-1.0||S-FeCoNi/NF-1.0 system after 500 h of operation at 100 mA cm^{-2}.

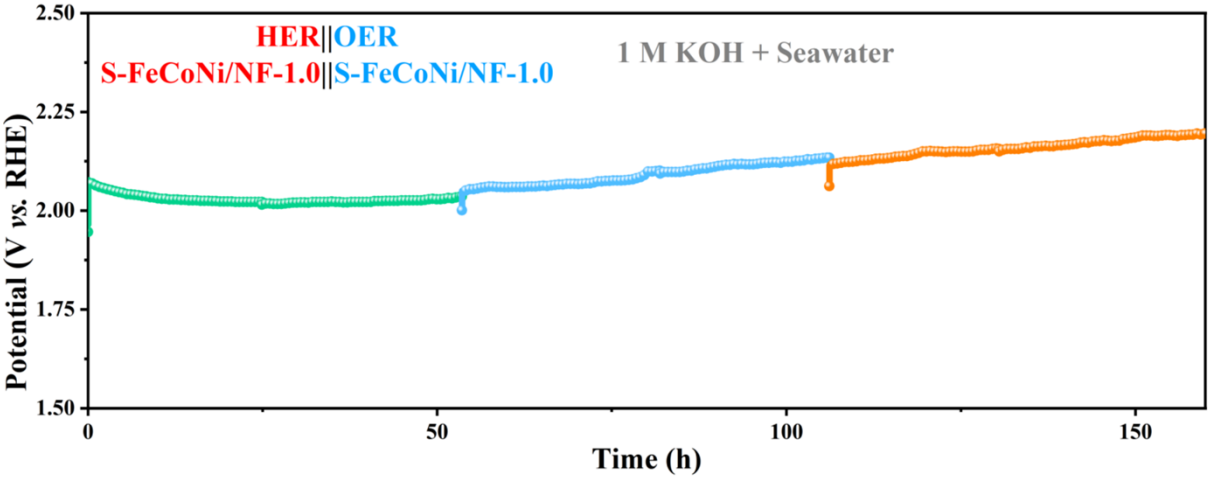

Figure S16. CP curves of 200, 300, and 400 mA cm^{-2} for 50 h.

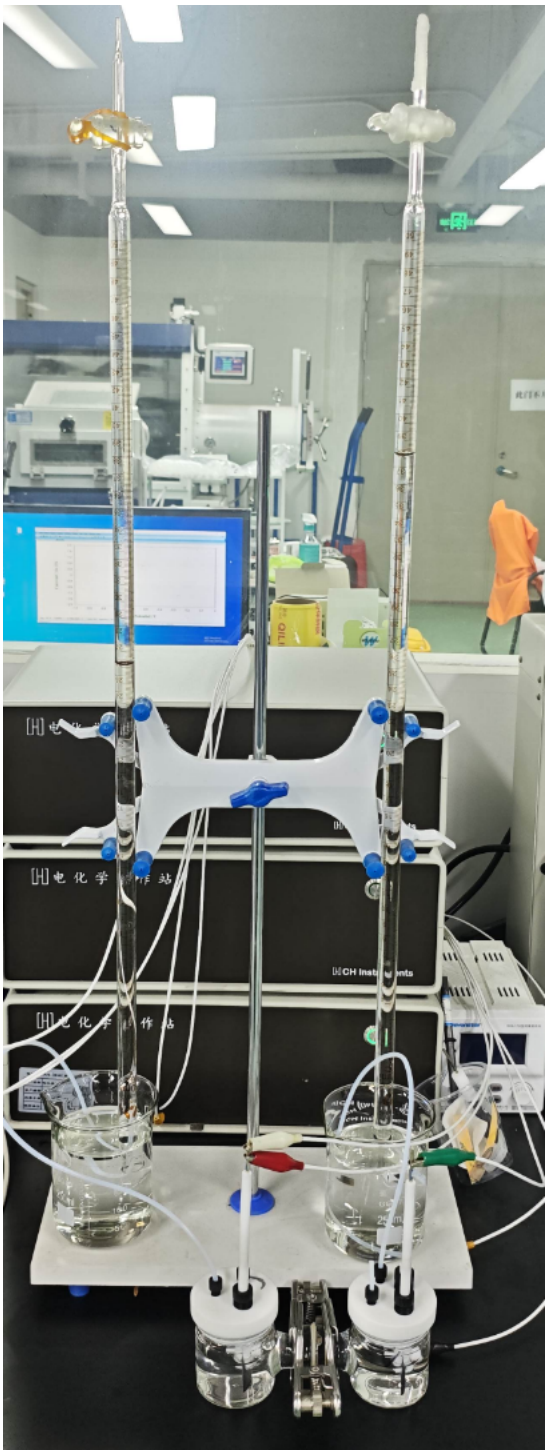

Figure S17. Devices for measuring Faraday efficiency of H_2 and O_2 product in the HER||OER alkaline seawater splitting system.

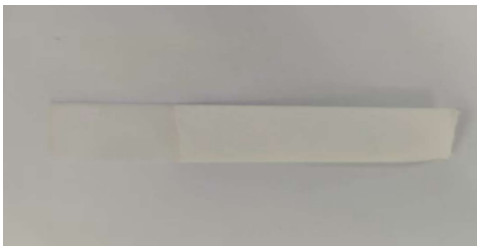

Figure S18. The relationship between the colour change of starch iodide paper and the alkaline seawater electrolyte after the HER||OER stability test (500 h@0.1 A cm^{-2}).

Table S1 Comparison of R_{ct} values obtained from equivalent electrical circuit of S-FeCoNi/NF-1.0 and control samples in alkaline seawater electrolytes for HER.

Catalyst	R_s (Ω)	R_{ct} (Ω)	CPE-T	CPE-P
PtC	1.13	0.49	7.14×10^{-4}	8.16×10^{-1}
S-FeCoNi/NF-1.0	0.86	1.82	4.82×10^{-1}	7.30×10^{-1}
S-FeCoNi/NF-0.5	0.96	2.26	2.21×10^{-1}	7.69×10^{-1}
S-FeCoNi/NF-1.5	0.95	3.99	2.90×10^{-1}	7.05×10^{-1}
S-NF	1.18	4.66	2.41×10^{-3}	6.93×10^{-1}
FeCoNi/NF	1.06	5.00	7.97×10^{-3}	7.29×10^{-1}

R_s is solution resistance, R_{ct} is charge transfer resistance, CPE is constant phase element.

Table S2 Comparison of R_{ct} values obtained from equivalent electrical circuit of S-FeCoNi /NF-1.0 and control samples in alkaline seawater electrolytes for OER.

Catalyst	R_s (Ω)	R_{ct} (Ω)	CPE-T	CPE-P
RuO_2	0.82	3.20	4.59×10^{-2}	8.23×10^{-1}
S-FeCoNi/NF-1.0	1.08	1.13	2.71	6.89×10^{-1}
S-FeCoNi/NF-0.5	0.97	2.10	2.55	7.60×10^{-1}
S-FeCoNi/NF-1.5	1.17	2.15	1.66	5.90×10^{-1}
FeCoNi/NF	1.16	2.31	7.43×10^{-2}	7.89×10^{-1}
S-NF	0.98	4.07	6.11×10^{-2}	7.58×10^{-1}

R_s is solution resistance, R_{ct} is charge transfer resistance, CPE is constant phase element.

Table S3 A comparison of the HER performance of the S-FeCoNi/NF-1.0 developed in this study with that of other recently reported materials.

Catalyst	Electrolyte	Overotential@ Current Density (mV@mA cm^{-2})	Stability (mA cm^{-2}@h)	Reference
S-FeCoNi/NF-1.0	1 M KOH + seawater	188@50 211@100	100@60	This work
$Fe_{1.0}Co_{1.1}Ni_{1.4}$-NC	1 M KOH	175@10	30@10	J. Mater. Chem. A, 2020, 8, 9021-9031
Ni-WO_x@NF	1 M KOH + seawater	45.69@10	10@120	Appl. Catal. B Environ., 2023, 325, 122397.
2D meso-Mo_2C/Mo_2N	1 M KOH + seawater	197@10	10@20	Angew. Chem. Int. Ed., 2022, 61, e202112298.
Ti/TiO_2@NiB_x	1 M KOH + 0.5 M NaCl	91@10	500@72	Chem. Eng. J., 2022, 430, 132881.
Ni-SA/NC	1 M KOH + seawater	139@10	200@14	Adv. Mater., 2021, 33, 2003846.
RuIr	1 M KOH + seawater	75@10	10@100	Small, 2024, 20, 2405784.

Table S4 A comparison of the OER performance of the S-FeCoNi/NF-1.0 developed in this study with that of other recently reported materials.

Catalyst	Electrolyte	Overpotential@ Current Density (mV@mA cm^{-2})	Stability (mA cm^{-2}@h)	Reference
S-FeCoNi/NF-1.0	1 M KOH + seawater	214@50 224@100	100@60	This work
$Fe_{1.0}Co_{1.1}Ni_{1.4}$-NC	1 M KOH	270@10	10@21	J. Mater. Chem. A, 2020, 8, 9021-9031.
Ti/TiO_2@NiB_x	1 M KOH + 0.5 M NaCl	338@10	10@72	Chem. Eng. J., 2022, 430, 132881.
FeMn-MOF	1 M KOH + seawater	255@100	100@100	Adv. Funct. Mater., 2025, 36, e08413.
MnO_x/NiFe-LDH/NF	1 M KOH + 0.5 M NaCl	265@100	50@70	Inorg. Chem., 2022, 61, 15256-15265.
NiS_x/$BaNiO_3$	1 M KOH + 0.5 M NaCl	350@50	50@12	Chem. Eng. J., 2025, 515, 163612.
NiFe-LDH/V_2CT_x/NF	1 M KOH + 0.5 M NaCl	241@100	500@110	Nano Materials Science, 2024, 6, 413-418.

Table S5 Comparison of the HER||OER electrolytic system assembled using the S-FeCoNi/NF-1.0 bifunctional catalyst developed in this study with other recently reported works.

Catalyst	Electrolyte	Potential@ Current Density (V@mA cm^{-2})	Stability (mA cm^{-2}@h)	Reference
S-FeCoNi/NF-1.0	1 M KOH + seawater	1.642@50 1.722@100 1.814@200	100@500	This work
Fe_3O_4@Ni_3S_2	1 M KOH + seawater	1.58@10	50@30	Chem. Eng. J., 2024, 501, 157628.
Ni/Cr_2O_3@P-RuO_2	1 M KOH + seawater	2.0@1500	100@500	Adv. Funct. Mater., 2026, e75248.
RuMoNi	1 M KOH + seawater	1.82@1000	100@240	Nat. Commun., 2023, 14, 3608.
$NiCoP_v$@NF	1 M KOH + seawater	2.43@500	500@120	Adv. Energy Mater., 2024, 14, 2400975.
NiFeS/NF	1 M KOH + seawater	1.67@100 1.85@500	100@25 500@25	J. Mater. Chem. A, 2023, 11, 1116-1122.
Mo-CoP_3@FeOOH	1 M KOH + seawater	1.83@100	1.69 to 1.72 V@350	Small Methods, 2024, 8, 2301474
NNNF@Mo_2N/FeO_xN_y	1 M KOH + seawater	1.47@20	100@100	Chem. Eng. J., 2024, 489, 151348.

Reference

[1] Nat. Commun., 2018, 9, 4365.

[2] Int. J. Hydrogen Energy, 2024, 90, 747-756.